# A COMPREHENSIVE ANALYSIS OF THREE-DIMENSIONAL NORMAL GRAIN GROWTH OF PURE IRON VIA MULTI-PHASE FIELD SIMULATION

## H. Mao [a], B. Li [b*], Y. Du [a]

[a] State Key Laboratory of Powder Metallurgy, Central South University, Changsha, China
[b] College of Mechanical and Power Engineering, China Three Gorges University, Yichang, China

*Abstract*

*A three-dimensional (3D) multi-phase field model was established to simulate normal grain growth in pure iron. The advanced visualization technology was used to extract the related data for individual grains, which can clearly display the grain morphology with distinct grain boundary surface as well as the space distribution of neighboring grains. Based on the simulation results, the grain growth kinetics model was described, which is in conformity with Burke and Turnbull's parabolic law. The phenomenon of a 'Hillert regime' in 3D grain growth and the topological transformation mechanism were investigated. The grain size distributions under different time evolution showed a good agreement with the Hillert distribution. The details of grain growth, especially grain size distribution and volume growth rate, were analyzed. The models of von Neumann-Mullins and Hilgensfeldt for predicting the volumetric growth rate were compared. The volumetric growth rate was approximately zero when the number of grain sides was close to 13.7. The multi-phase field simulation can be used to analyze the dynamic evolution of the topological relationship of grains and reveal the general law of normal grain growth quantitatively.*

*Keywords: Grain growth; Multi-phase field model; Grain size distribution; Topological analysis*

## 1. Introduction

The grain growth law is one of the important issues in materials science research, which determines the final microstructure and mechanical properties of polycrystalline material. As is well known, the grain growth is a rather complex multi-physical phenomenon. Clarifying the mechanism of grain growth during materials processing is one of the key scientific issues that researchers have tried to solve [1]. Over the past decades, researches on grain growth mainly focused on two aspects: theory and experiment. Experimental investigations have been widely used to study the grain growth of different materials. However, relying on experimental methods will be expensive and time consuming, and it is difficult to obtain dynamic evolution information. On the other hand, computer simulation is an important tool to investigate grain growth. For polycrystalline materials, computer simulation about grain growth evolution can not only visually show its dynamic evolution process, but also provide a quantitative analysis about topological characteristic and systematic investigation of the dynamics of grain growth [2].

Monte Carlo-Potts model, Vertex dynamics model, Cellular Automaton, Level-set method [3] and phase-field model are different numerical approaches to simulate grain growth [4, 5]. In 1984, Monte Carlo method was firstly used to study normal grain growth process by Srolovitz et al [6]. Since the early 1990s, Hesselbarth et al [7] have simulated the recrystallization process by cellular automata model. Recently, the application of cellular automata model in recrystallization and grain coarsening has been developed rapidly. Weiaire et al [8] established the vertex model to simulate a two-dimensional grain evolution process. It is worth noting that phase-field crystal model can capture the dislocation networks that form grain boundaries, and give rise to anisotropic dissolution kinetics, as described by Yamanaka et al [9]. Compared with these numerical simulation methods, phase field model that has been developed in recent years is considered to be the most promising method to quantitatively describe grain growth. The phase field method shows significant advantages in modelling the microstructure evolution in which the thermodynamic and kinetic data can be taken into account, such as Gibbs free energy, grain boundary mobility, elastic anisotropy and so on. For the evolution of complex microstructures, the unique definition of the grain boundary by the phase field equation makes it unnecessary to track the interface

---

all the time, and can complete large-scale simulations while improving efficiency. The phase field method has been successfully applied in many fields such as dendrite growth, rafting process, and the second phase precipitation [10, 11]. Zhu [12] studied the g¢ precipitate microstructure evolution in a nickel based high temperature alloy in 3D phase-field simulation with coupling CALPHAD (Computer Coupling of Phase Diagrams and Thermochemistry) database. Reza and Steinbach [13] investigated the features of grain growth about topological properties and mean-field approximation by using multi-phase-field model.

As an average field theory, Hillert grain growth theory is widely accepted among various grain growth modes, and it is believed that the grain growth process is a dimensional flow process. The growth or reduction of individual grains depends entirely on their critical sizes. The topological characteristics of grain growth, such as the morphology and volume fraction of grain boundaries, the smoothness of the interface, and other two-dimensional defects that affect the movement of dislocations, will ultimately decide the material properties [14]. Wakai et al. [15] investigated topological transformations of grain growth by Surface Evolver method. Weygand et al. [16] used vertex models to simulate the evolution of 3D grain structure. However, there have been limited investigations about 3D single grain dynamic structure evolution using multi-phase field model. Meanwhile, there are also few reports about topological transformations of 3D grain growth.

In this work, the major purpose is to study microstructure evolution during 3D grain growth in pure iron by using multi-phase-field model. The advanced visualization programs are developed to analyze the grain morphology and its evolution behavior precisely. The existence of a 'Hillert regime' in 3D grain growth and the topological transformation mechanism are also investigated. Furthermore, the relationship between the volumetric growth rate and the normalized grain radius is studied.

## 2. Theory and Model Description
### 2.1 Grain Growth Theory

The classical model for normal grain growth proposed by Burke and Turnbull [17] deduces a parabolic relationship for grain evolution. In this model, it is assumed that the grain boundary migrates toward the centre of its curvature, which in turn reduces the interfacial area as well as its associated energy.

$$v = \mu_{ij} \cdot P = \mu_{ij} \cdot \sigma_{ij} \cdot \left( \frac{1}{r_1} + \frac{1}{r_2} \right) \tag{1}$$

$$P = \sigma_{ij} \cdot \left( \frac{1}{r_1} + \frac{1}{r_2} \right) \tag{2}$$

where $s_{ij}$ and $m_{ij}$ represent surface energy and grain boundary mobility, respectively; P is driving force; $r_1$ and $r_2$ are the two principle curvatures of the surface. The growth rate (dA/dt) of individual grains in the model can be described by the von Neumann-Mullins law [18]:

$$\frac{dA}{dt} = -\mu_{ij}\sigma_{ij}\frac{\pi}{3}(6-f) \tag{3}$$

where A is the area of grain, and $f$ is the number of sides, or the number of adjacent grains for each grain. Two different development trends for grain evolution can be determined by the number of sides. If the number of sides is greater than 6, the grains grow; and if below 6 the grains shrink.

A critical grain size introduced by Hillert in 1965 dictates the growth or shrink of grains [19]. Starting from Eqs. (1) and (2), Hillert managed to introduce that the growth rate of small grains is negative and that is positive for large grains:

$$\frac{dR}{dt} = K\left( \frac{1}{R_{Cr}} - \frac{1}{R} \right) \tag{4}$$

Here, K is equal to $as_{ij}m_{ij}$ (a is a constant), and the critical grain size, $R_{cr}$, is related to the instantaneous average grain size, which varies with time evolution.

The stability condition of Lifshitz-Slyozov (LS) is also an important analysis index of grain evolution. Hillert successfully used this model to solve the particle coarsening problem [20]. All predictions in the Hillert theory are rigorously derived from Eq. (4), which can be listed as follows [21]. First, the square of the average grain size $\langle R(t) \rangle^2$ is a linear function of time:

$$\langle R \rangle^2(t) - \langle R \rangle^2(0) = kt \tag{5}$$

where $\langle R(0) \rangle$ is the initial average grain size and k is a constant.

The critical radius $R_{cr}$ is given by

$$R_{Cr} = \frac{9}{8}\langle R \rangle \tag{6}$$

The above equations show that if the grain radius R is greater than $R_{cr}$, it will grow up, while the others shrink. And the final grain size distribution at the steady state is given by

$$F_{(\rho)} = (2e)^3 \frac{3\rho}{(2-\rho)^5} \exp\left( -\frac{6}{2-\rho} \right) \tag{7}$$

where $r=R/R_{cr}$. In the present work, the Hillert 3D theory was used to test all assumptions and predictions.

### 2.2 Topological illustration of grain growth

Many analytical approaches, which depend on the

topological characteristics of the grains and, particularly, on the number of faces or the topological class of a grain, have been used to describe the growth rate of 3D grains growth. Among them, a corresponding 3D growth law proposed by Mullins [22] assumed that grains are regular polyhedral. Glazier [23] established the relationship between the growth rate and the number of faces of polyhedral grain with the time evolution. Based on these findings, more elaborate statistical versions of this 3D von Neumann have been proposed and compared with the simulation results of the Surface Evolver program [24]. In this work, we compared the growth rates from the phase field simulation with the previous versions of the 3D law.

The general form of the 3D von Neumann law can be described as

$$V^{-1/3}\frac{dV}{dt} = 2\mu\sigma G(f) \tag{8}$$

where $V$ and $f$ are the grain volume and the number of faces per grain respectively. In the Mullins' approach, the function G($f$) is given by

$$G(f) = \frac{1}{2}\left(\frac{3}{4\pi}\right)^{1/3} G_1(f) G_2(f) \tag{9}$$

$$G_1(f) = \frac{\pi}{3} - 2\tan^{-1}\left(\frac{1.86(f-1)^{1/2}}{f-2}\right) \tag{10}$$

$$G_2(f) = 5.35 f^{2/3}\left(\frac{f-2}{2(f-2)^{1/2}} - \frac{3}{8}G_1(f)\right)^{-1/3} \tag{11}$$

More recently, Hilgenfeldt et al. [25] proposed a similar model depending on geometrical features of convex bodies, specifically on the caliper radius, which also has a close relationship with the mean curvature [26]. They found that the normalized volume rate of change is given by:

$$\left(\frac{dv}{dt}\right)V^{1/3} = \mu\sigma G_H(f) \tag{12}$$

$$G_H(f) = \frac{3\left[(f-2)\tan\pi/\eta_f\right]^{2/3}\tan^{1/3}(\chi_f/2)}{2^{1/3}}\left(\frac{\pi}{3} - \chi_f\right) \tag{13}$$

$$\eta_f = 6 - \frac{12}{f} \tag{14}$$

$$\chi_f = 2\cdot\arctan\left\{\left[4\cdot\sin^2\left(\pi/\eta_f\right)^{1/2}\right]\right\} \tag{15}$$

### 2.3 Multi-Phase Field Model

The driving force that plays an important in the growth of the grain and the total energy landscape comprises of bulk free energy and the interfacial energy. The variation form of phase-field equations

ensures that the total energy is minimized. In pure iron, this is going to be entirely governed by the minimization of interfacial energy. In the multi-phase-field model, each individual grain is described by its own phase-field variable $f_i$, i=1,...,N. In the bulk of grain i, $f_i$=1 and $f_i$=0 represent other region [27]. The change of phase field variable $f_i$ at the grain boundary is continuous and smooth transition, and the value is 0~1. The N phase-field variables are correlated with the constraint $\sum_{i=1}^{N}\phi_i = 1$. For normal grain growth, the total free

$$F = \int_V f^{\text{intf}} dV \tag{16}$$

The interfacial energy density of system described by Steinbach and Pezzolla [27] is given as following

$$f^{\text{intf}} = \sum_{i=1,i\neq j}^{N}\frac{4\sigma_{ij}}{\eta}\left\{-\frac{\eta^2}{\pi^2}\nabla\phi_i\cdot\nabla\phi_j + \phi_i\cdot\phi_j\right\} \tag{17}$$

where, again, $s_{ij}$ and $m_{ij}$ are the grain boundary energy and mobility between i and j grains, and h is the interface width. In the actual material system, both the anisotropy energy of grain boundary and the misorientation between neighbor grains affect the grain growth [28]. However, for an ideal system, it is assumed that the two former parameters ($s_{ij}$ and $m_{ij}$) are equal for all pairs of grains, and the curvature of grain boundary is the main driving force for grain growth.

Therefore, the microstructural evolution of the system can be described by the evaluation of the phase variables. This is given within a generalized form of the Ginsburg-Landau equation:

$$\dot{\phi}_i = \sum_{j=1}^{N}\frac{\mu_{ij}}{N}\left(\frac{\delta F}{\delta\phi_i} - \frac{\delta F}{\delta\phi_j}\right) = \frac{\mu_{ij}\sigma_{ij}}{N}\sum_{j=1\neq i}^{N}\left[I_i - I_j\right] \tag{18}$$

$$I_\gamma = \nabla^2\phi_\gamma + \frac{\pi^2}{\eta^2}\phi_\gamma \tag{19}$$

Here $N$ is the local number of grains (N=2 for grain boundary, N=3 for triple junction, and so on).

In our work, pure iron was chosen as the simulation target system. The surface energy in pure Fe $s_{ij}$ =1.35J m$^{-2}$, and boundary mobility $m_{ij}$ =5.53×10$^{-17}$ m$^4$J$^{-1}$S$^{-1}$ were taken from the literature [29-33]. The simulation domain was 512′512′512 grid points with a grid spacing of Dx=1×10$^{-6}$ m, and interfacial width h=6Dx. The initial grain structure wascreated by allowing 12000 grains created with a Voronoi tessellation to grow in an undefined polycrystal. Figure 1 presents structure evolution after 1500, 3500, and 5500 time steps. As shown in Fig.1, with evolution time, the average grain size increases significantly. It can be also concluded that the angle at the junction of the trigeminal crystal is close to 120°, and most of the grain boundaries are smoothly curved.
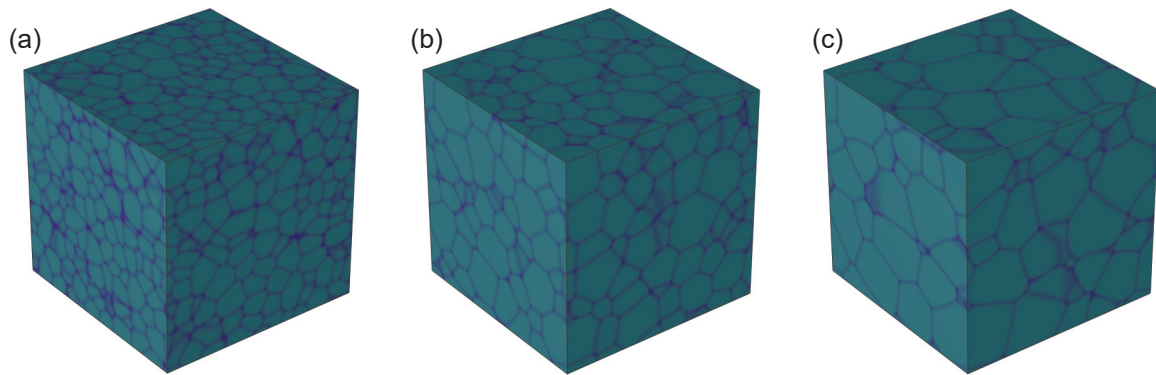
Since actual metal materials are opaque

***Figure 1.** Polycrystalline structure evolution of pure iron at different simulation time steps by using 3-D phase field method. The simulation box is 512Δx×512Δx×512Δx.(a) 1500 time steps; (b) 3500 time steps; (c) 5500 time steps*

materials, the three-dimensional individual grains cannot be observed directly. In order to get the three-dimensional grain size and morphology, the advanced visualization technology was used to extract the individual grain data to study the geometric shape and topological structure, and the 3D individual grain morphology was observed from multi-view observation. Figure 2 shows the three-dimensional grain morphology with evolution time, and the shape, spatial position, grain boundary, and tricrystalline edge of a single grain are quite clear in this series of results. It is also convenient to display more than one 3D grain at a given viewing angle. In 3D space observation, it is helpful to eliminate the misjudgment that may occur in 2D observation. The incomplete grains contacted with the surface were removed in order to display intact grains clearly. It can also clearly demonstrate that the three-dimensional geometric morphology of different grains and their spatial position relationship with each other. Due to an accurate reconstruction of geometric features such as concave and convex grain interfaces and tricrystalline edges, it also lays a foundation for the subsequent accurate measurement of important parameters such as interface curvature and tricrystalline edge length.

In this work, the pure iron was used to set as the benchmark test. The parameters used in the simulation are shown in Table 1.

### 3. Results and discussion
### *3.1 Kinetics of Grain Growth*

Figure 3 indicates the changes of grain numbers and average grain sizes as a function of time steps. It can be easily found that there are three regions during the whole simulation process. In order to ensure the validity and reliability of statistics, the initial state has set 12000 initial grains in the simulation area. It can be observed from the Fig.3 (a) that the number of grains decreases sharply in the first stage. Subsequently, the grain numbers gradually decrease

with the evolution of time steps in region 2, the minimum grain numbers were 1080 at 14800 time steps in region 2. In region 3, the number of grains decreased from 1080 to 1020. The reduction rates of the number of grains in the latter two stages are significantly lower than that in the first stage. In the third stage, the number of grains tends to stabilize. As shown in Fig.3 (a), there is an inverse correlation between grain size and number. The grain size (radius of grain) gradually increased with the evolution of time. These conclusions are consistent with the general law of grain growth.

The simulation process well conforms to the following parabola equation of normal grain growth:

$$\langle R_t \rangle = \left[ K(t - t_0) + \langle R_0 \rangle^{\frac{1}{n}} \right]^n \tag{20}$$

in which $\langle R_0 \rangle$ represents the initial average grain size, $t_0$ the initial moment, and $\langle R_t \rangle$ the average grain size at time t. K is a constant. After calculation, we know that the grain growth index n=0.501 during the whole grain growth process in Fig. 3(a), which is almost the same as the theoretical value n=0.5 of the grain growth index.

Figure 3(b) indicates the changes of the squared mean grain sizes as a function of time steps. It can be easily observed that there is a good linear relationship between the squared mean grain sizes and time steps, indicating the parabolic kinetics of grain growth. According to Fig. 3(b), a parabolic equation can be obtained as:

$$\bar{R}^2 \left[ m^2 \right] = 0.022 * t + 19.33 \tag{21}$$

Figure 4 shows the relationship between the volumetric growth rate and the normalized grain radius. The different colors indicate the topological classes. The shape of the distributions shows a good agreement with the function obtained from the mean-field approximation. The most prominent relative sizes can be easily estimated from a volumetric perspective according to the following expression [26]:
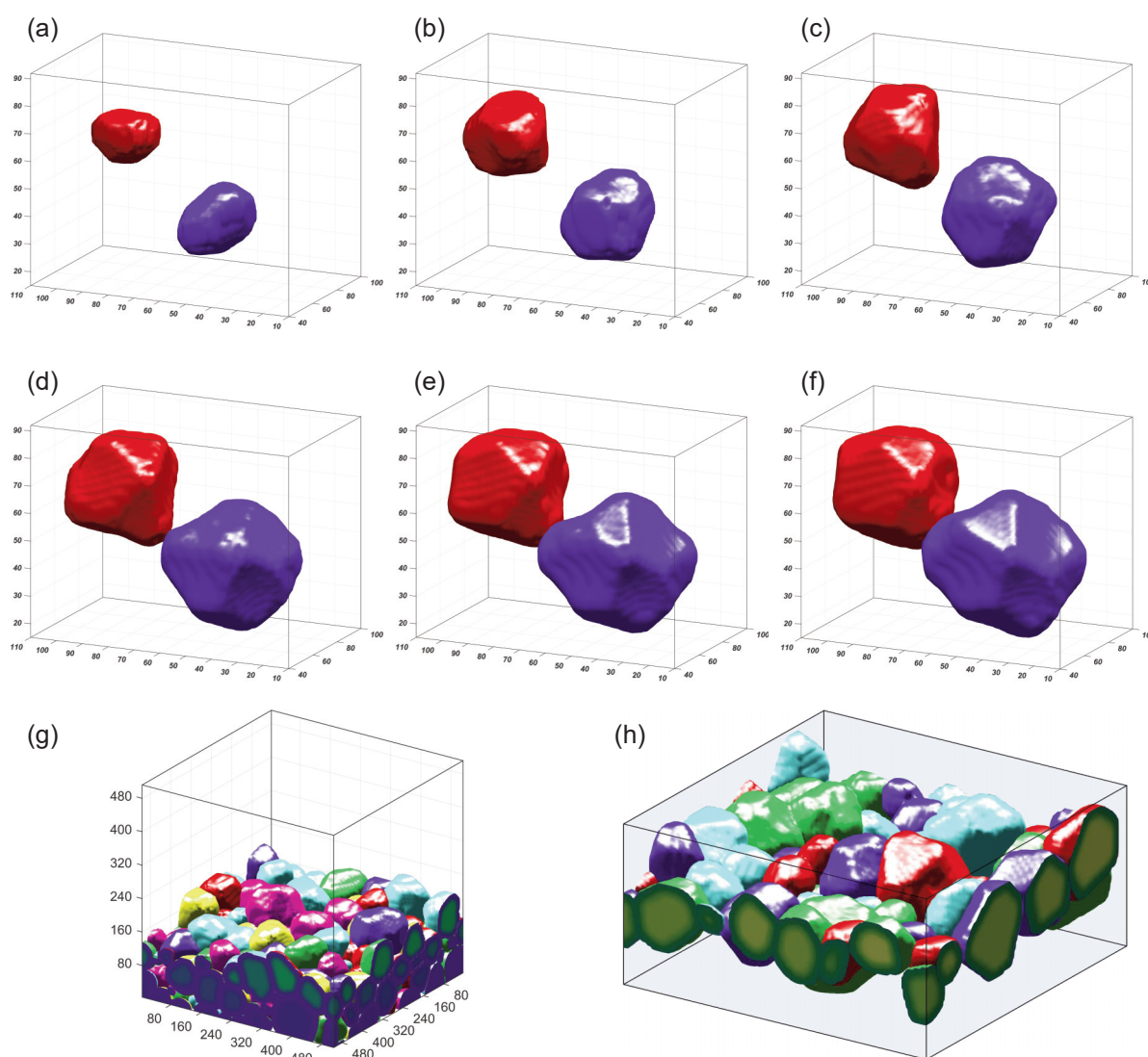
***Figure 2.*** *The evolution of two grains from small sizes to their grain boundaries contact at growth process in 3-D phase field simulation (different color indicates different orientation of grain). (a)100 time steps;(b) 1000 time steps; (c) 2000 time steps; (d) 3000 time steps; (e) 3500 time steps; (f) 4000 time steps. (g) the multi-layer grain structure obtained by 3-D phase field simulation; (h) the single-layer grain structure obtained by 3-D phase field simulation*

***Table 1.*** *Parameters used in the multi-phase field simulation*

| Parameters | Symbols | Values |
|---|---|---|
| Grid spacing | $\Delta x$ | $1 \times 10^{-6}$ m |
| Initial time step | dt | $1 \times 10^{-5}$ s |
| Interface width | $\eta$ | $6 \times 10^{-6}$ m |
| Interface energy | $\sigma_{ij}$ | 1.35 J m$^{-2}$ |
| Boundary mobility | $\mu_{ij}$ | $5.53 \times 10^{-17}$ m$^4$J$^{-1}$S$^{-1}$ |

$$\frac{\mathrm{d}V}{dt} = SR^2 \frac{\mathrm{d}R}{dt} \tag{22}$$

where S is a shape factor, which is equal to $4\pi$ for spherical particles. From the mean-field theory, the fastest shrinkage rate was predicted to be $0.5R_{cr}$ [13]. This is also comparable with simulation results obtained from Kamachali et al [13], who also investigated the relationship between the growth rates of individual grains and the grain sizes, and obtained the similar results with our works. The shape of the distribution changes slightly with the evolution of time.
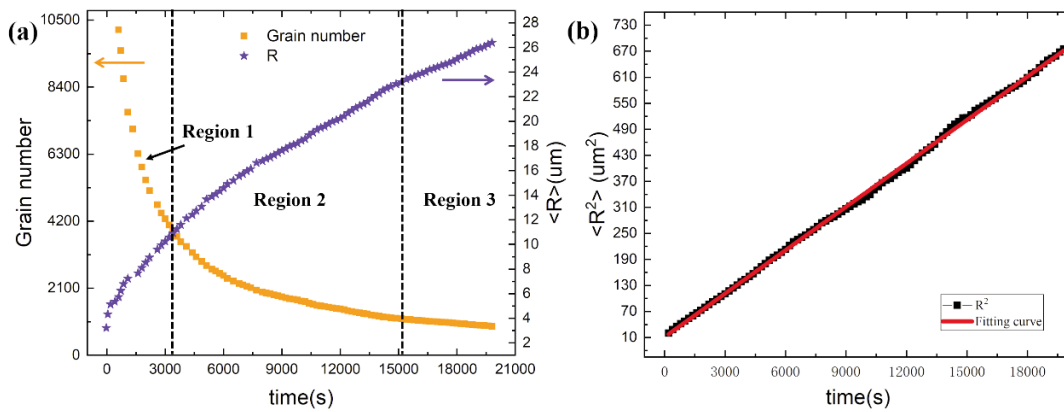
***Figure 3***. *(a) The relationship between the number of grains and the average grain radius as a function of evolution time in phase field simulation;(b) Linear function of average grain area and evolution time during grain growth*
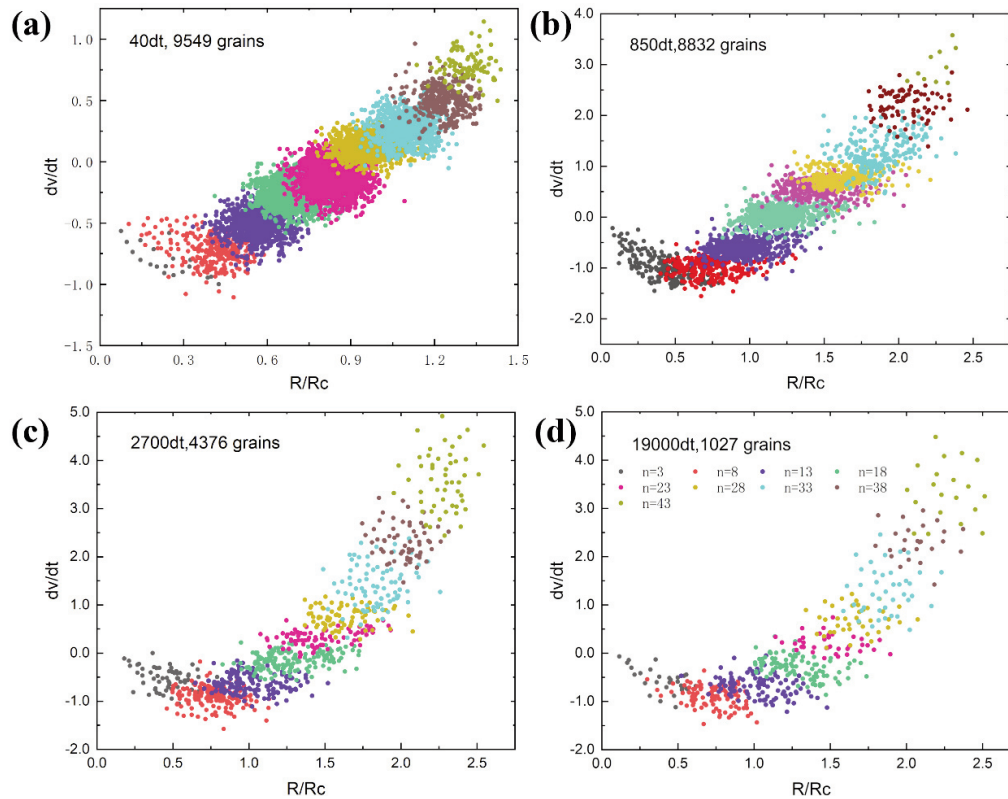


***Figure 4.*** *The changes of volumetric rate for different time steps. The color coding relates to the topological classes n. (a) 40 time steps, 9549 grains; (b) 850 time steps, 8832 grains; (c) 2700 time steps, 4376 grains;(d) 19000 time steps, 1027 grains*

### 3.2 Grain size distribution

In order to make sure the reliability of the statistical results, the initial grain numbers were set to be 10000 to investigate the grain sizes distribution. **Figure 5** indicates the grain size distribution under different time steps.

As shown in Fig.5a, at the initial stage, the grain sizes distribution is very narrow. With the increasing of time steps, there is a broader distribution at 3000

time steps. Meanwhile, it can also be easily found that the grain size distribution begins to gradually match the Hillert distribution [19]. The grain size distribution almost closely matches the Hillert distribution (Fig.5b), and begin to keep a stable state for a long time. The grain size distributions present a typical symmetric distribution. During this period of grain growth, the grain numbers decrease slowly from 3522 to 2138. As seen in Fig.5c, the peak of the distribution moves to the left side of the Hillert

distribution gradually. The grain distribution basically meets the Hillert distribution with only a little bit of volatility (Fig.5d). Although the grain size distribution basically matches the Hillert distribution, there is still a little deviation between the phase-field simulation results and Hillert¢s prediction. The reduction rate of grain numbers become less gradual. The symmetric distribution can still be observed. The results show that the whole grain sizes distribution of the simulations fulfils the self-similarity regularization.

Figure 6 is the variation of the average grain face number with time evolution. It can be seen that during the transition stage (0~2000 time steps) and the growth stage (2000~10000 time steps), the average grain face number <f> increases with evolution time, showing a monotonic and increasing curve relationship. At the quasi-steady state stage (10000 to 20000 time steps), the average grain face number <f> floats around 13.7 and that is very close to the one from ref [25]. The average grain face number at different times of annealing at 635°C was measured using a series of cross-sectional methods [34]. It was found that with the extension of the annealing time, the average grain face number <f> gradually approached a certain value from about 9.5. It is close to 13 when annealing 10 min.

Figures 7(a) and 7(b) are the evolution of grain face number distribution. It can be seen that the distribution of the grain numbers is basically unchanged during the transition stage, which is the parameter μ=11.67, σ=0.35 lognormal distribution, at the peak of f=10; After 3400s, as shown in Fig. 7(b),
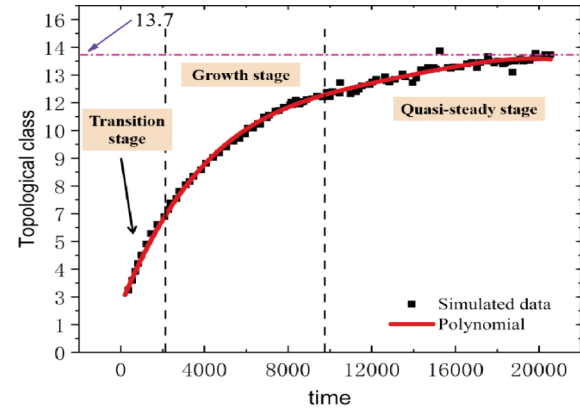


***Figure 6.*** *Variation of topological class of average grains with time evolution. It can be divided into three stages: transition stage (0-2000 time steps), growth stage (2000-10000 time steps) and quasi-steady stage (10000-20000 time steps). The final topological class for average grains will be stable around 13.7*
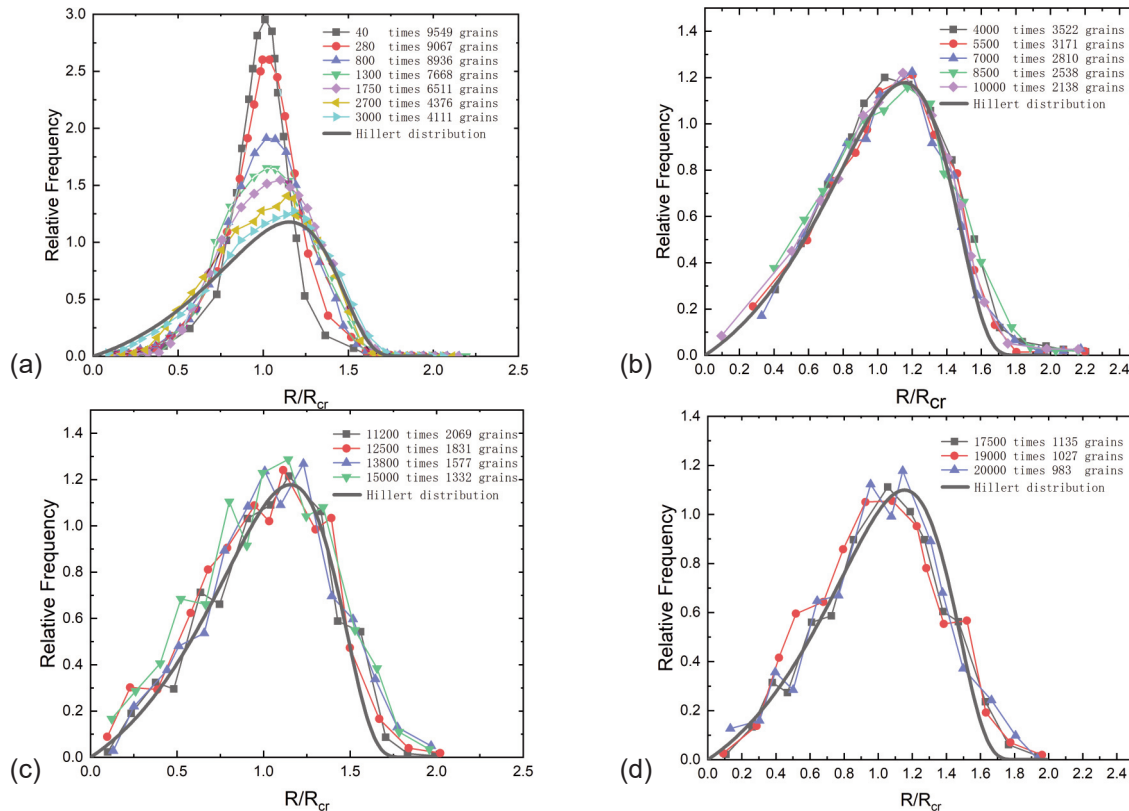


***Figure 5.*** *Grain distribution at different time evoluation of the grain growth. The solid black lines represent the Hilliert distribution of the grain growth. (a) Grain growth from 40 to 3000 time steps, (b) 4000 to 10000 time steps, (c) 11200 to 15000 time steps, (d) 17500 to 20000 time steps*

the peak face number distribution is still at f=10, but the peak strength gradually increases, and the surface number distribution is no longer self-similar. Therefore, it can be concluded that the number distribution of grains has self-similarity between the transition stage and the quasi-steady growth stage. At the end of the quasi-steady state stage, the face number distribution no longer has self-similarity. In terms of individual grains, the minimum interface number obtained by this simulation is 3; the maximum interface number $f_{max}$ is 43. The number of individual grains measured by experiments during the growth of aluminum grains in pure Al is 3 to greater than 50 [35] Therefore, the simulation results are similar to those observed in real materials.

### 3.3 3-D Von Neumann–Mullins Law

As shown in Fig.8a, there is a comparison between the change rates of grain area dA/dt and the normalized grain radius R/Rc under different topological class. The color presents different topological classes. With the increasing of topological class, the change rate of grain area increases. The

main topological classes are focused on 10-30. It also can be easily found that the same color dots mostly stay on a horizontal line. Fig.8b indicates the change rate of grain area dA/dt plotted with topological classes. The error bars present the standard deviations. There is a typical linear relationship between dA/dt and topological classes. The straight line has a good agreement with von Neumann-Mullins.

Mullins [18, 22] and Hildefeldt et al. [25] investigated the relationship between topological class and the volumetric change rates of the grain growth, and they also supplied empirical function. Figure 9 presents the normalized volumetric change rate among the simulations and these theoretical formulas. At the initial stage of the grain growth, the simulation values match well with Mullins and Hildefeldt's prediction, and there was also a slight deviation with the increasing of topological class; the slope of the fitting curves decrease slowly with the evolution of time. The volumetric growth rate is approximately zero when the number of grain sides is 13.7.

Figure 10 shows the grain sizes distribution of topological class. The dark line represents the whole
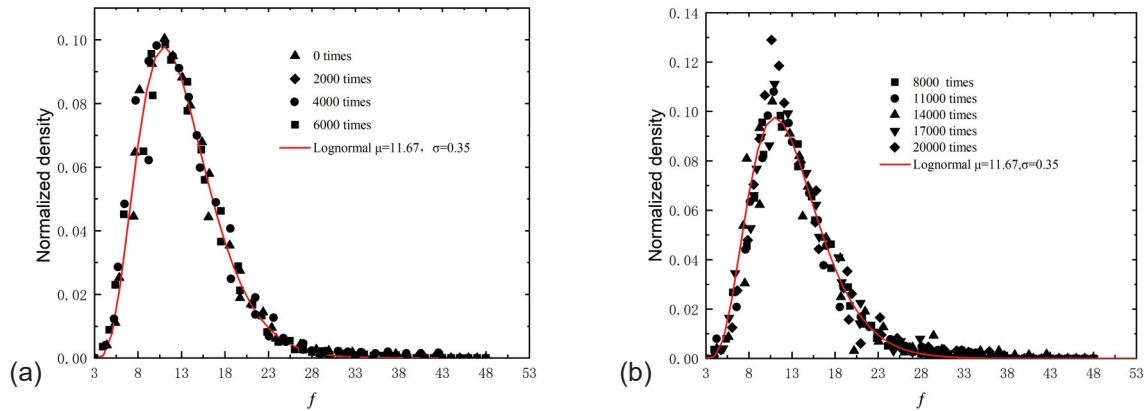


**Figure 7.** *The normalized density of grain with different face number under evolution: (a) 0-6000 time steps; (b) 8000-20000 time steps. The red solid lines represent the Lognormal distribution of topological class*
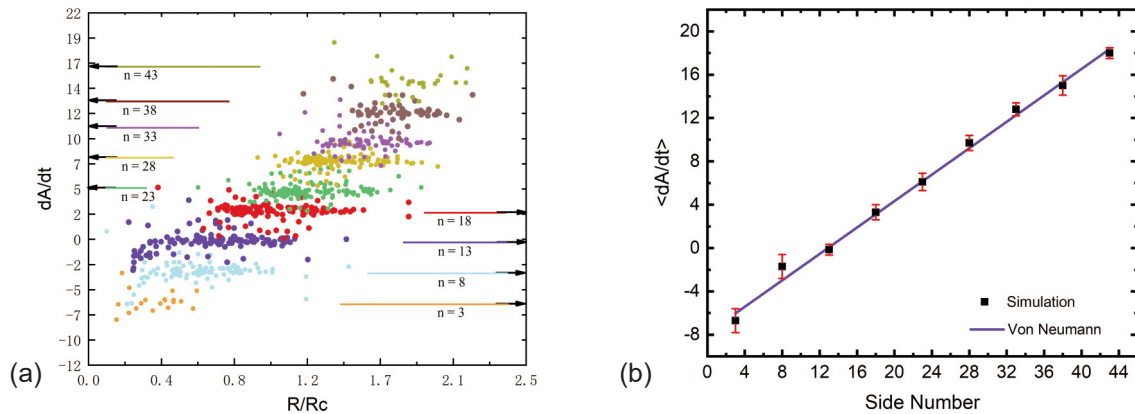


**Figure 8.** *(a) Area change rates dA/dt of 3485 individual grains plotted with the relative grain size (R/R_c) at 4500 time steps (n represents the face number of average grain). (b) Average area change rates <dA/dt> and their standard deviations plotted with the side numbers of grains*
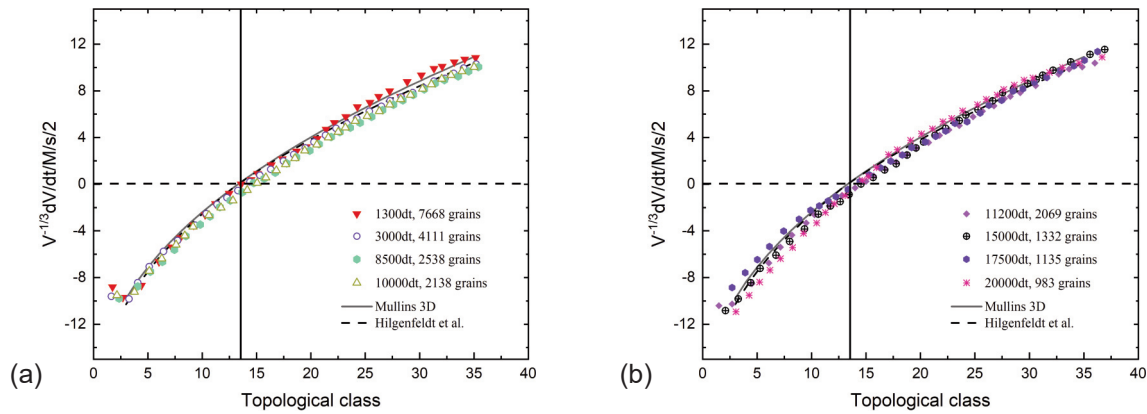
***Figure 9.*** *A comparison between normalized volumetric growth rate and the analytical expression. (a) the evolution time from 1300 time steps to 10000 time steps; (b) the evolution time from 11200 time steps to 20000 time steps. There is a good correlation between simulation results and the Mullins prediction. Our phase field simulation gives a value of around 13.7 for the neutral number*
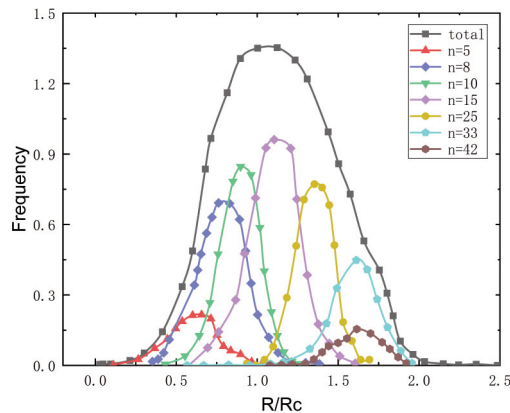


***Figure 10.*** *In the quasi-steady state of grain growth (20000 time steps), the distribution of each topological class of grains in phase field simulation*

simulations results. The other color lines show the grain sizes distribution of corresponding topological class, which was indicated by specific numbers. The grain size distribution presents a typical symmetric distribution at the symmetric axis of $R/R_c=1$. Meanwhile, with the increase of topological class, the grain sizes increase. When the topological class is 15 (purple line), there is also a typical symmetric distribution at $R/R_c=1$. It can directly reflect that the average grain side numbers mainly concentrated around 15.

## 4. Conclusion

In this work, the 3D grain growth was simulated by a multi phase-field model. The grain morphology with a distinct grain boundary surface as well as the space distribution of neighboring grains can clearly be displayed by the advanced visualization technology.
A parabolic equation was obtained, which is in conformity with Burke and Turnbull's parabolic law. The grain size distribution of the simulation results

matched well with the Hillert 3D distribution. The relationship between the topological class number and the relative grain size was also studied. In order to analyze the simulation results, the models of von Neumann-Mullins and Hilgensfeldt were applied to predict the volume change rate of grains. The present simulation results and these different models are basically consistent. The topological transformation mechanism of 3D normal grain growth was also investigated. The detailed time evolution of grain growth process is extracted, particularly topological class, the grain size distribution and the volumetric growth rate. The averaged volumetric growth rate is approximately zero when the number of grain sides is 13.7. In summary, the three-dimensional (3D) multi-phase-field model can simulate the normal grain growth process of pure iron accurately.

### Acknowledgement

### References

[1] J.A. Dantzig, M. Rappaz, Solidification. EPFL Press, Lausanne, Switzerland, 2009, p.1.

[2] B. Zhu, R. J. Asaro, P. Krysl, K. Zhang, J. Weertman, Acta. Mater.,54(12) (2006) 3307-3320.

[3] J. Furstoss, B. Marc, G. Clément, P. Carole, P. M. Daniel, Phys. Earth Planet In., 283 (2018) 98-109.

[4] L.Q. Chen, Scripta Metallurgica et Materialia., 32(1) (1995) 115-120.

[5] E. Miyoshi, T. Tomohiro, Comp. Mater .Sci., 112 (2016) 44-51.

[6] D.J. Srolovitz, M.P. Anderson, G.S. Grest, P.S. Sahni, Scripta Mater.,17(2) (1983) 241-246.

[7] Hesselbarth, W. Hanfried, I.R Göbel, Acta. Mater., 39(9) (1991) 2135-2143.

[8] D .Weaire, J.P. Kermode, Philos. Mag. B., 48(3) (1983) 245-259.

[9] A. Yamanaka, M. Kevin, P.W. Voorhees, Acta. Mater., 133 (2017) 160-171.

[10] X. Shuai, H .Mao, Y. Kong, Y. Du. J. Min. Metall. Sect. B-Metall., 53(3) (2017) 271-278.

[11] H. Mao, Y. Kong, X. Shuai, S. Tang, Y. Du, J. Min. Metall. Sect. B-Metall., 55(1) (2019) 101-110.

[12] J.Z. Zhu, Z.K. Liu, V. Vaithyanathan, L.Q. Chen, Scripta Mater., 46(5) (2002) 401-406.

[13] R.Z. Kamachali, I. Steinbach, Acta Mater., 60(6-7) (2012) 2719-2728.

[14] V. Yadav, N. Moelans, Scripta Mater.,142 (2018) 148-152.

[15] F. Wakai, Y. Shinoda, S. Ishihara, A Dominguez. J. Mater. Res., 16(7) (2001) 2136-2142.

[16] D. Weygand, Y. Brechet, J. Lepinoux, Philos. Mag. B., 78(4) (1998) 329-352.

[17] J.E. Burke, D. Turnbull, Progress in Metal. Physics.,3 (1952) 220–244.

[18] W.W. Mullins, J. App. Physics., 27(8) (1956) 900-904.

[19] M. Hillert, Acta Mater.,13(3) (1965) 227-238.

[20] I.M. Lifshitz, V.S. Vitaly, J. Physl. Cheml. Solids., 19(1-2) (1961) 35-50.

[21] J.B. Gao, M. Wei, L.J. Zhang, Y. Du, M. Liu, Y. Huang, Metall. Materl. Trans. A., 49(12) (2018) 6442-6456.

[22] W.W. Mullins, Acta. Mater., 37(11) (1989) 2979-2984.

[23] J.A. Glazier, Phys. Rev. Lett., 70(14) (1993) 2170-2173.

[24] R.H. Wu, Z.F. Yue, M. Wang. J. Alloy. Compd., 779 (2019) 326-334.

[25] S. Hilgenfeldt, M. Andrew, S.A. Koehler, H.A. Stone, Phys. Rev. Lett., 86(12) (2001) 2685.

[26] W. Mingtao, B.Y. Zong, G. Wang, J. Mater. Sci. Technol., 24(06) (2009) 829-834.

[27] I. Steinbach, F. Pezzolla, Physica. D., 134(4) (1999) 385-393.

[28] G. Abrivard, E.P. Busso, S. Forest, B. Appolaire. Philos. Mag., 92(28-30) (2012) 3618-3642.

[29] S. Ratanaphan, D.L. Olmsted, V.V. Bulatov, E.A. Holm, A.D. Rollett, G.S. Rohrer. Acta. Mater., 88(2015): 346-354.

[30] M.A. Tschopp, K.N. Solanki, F. Gao, X. Sun, M.A. Khaleel, M.F. Horstemeyer, Phys. Rev. B., 85(6) (2012) 064108.

[31] Z.B. Zhang, Y.B. Zhang, O.V. Mishin, N. Tao, W. Pantleon, D.J. Jensen. Metall. Mater. Trans A,47(9) (2016) 4682-4693.

[32] M.J. Santofimia,JG Speer, A.J. Clarke, L. Zhao, Jl Sietsma. Acta Mater., 57(15) (2009) 4548-4557.

[33] M. Pang, Y. Peng, P. Zhou,Y. Du, J. Min. Metall. Sect. B-Metall., 54(1) (2018) 111-118.

[34] F.N. Rhines, K.R. Craig, R.T. Dehoff, Metallurgical Transactions., 5(2) (1974) 413-425.

[35] G.Q. Liu, H.B. Yu, W.Q. Li, Acta Stereol., 1994, 13(2): 281-286.

# OPSEŽNA ANALIZA TRODIMENZIONALNOG NORMALNOG RASTA ZRNA ČISTOG ŽELEZA UZ POMOĆ SIMULACIJE VIŠEFAZNOG POLJA

**H. Mao [a], B. Li [b*], Y. Du [a]**

[a] Glavna državna laboratorija za metalurgiju praha, Centralno-južni univerzitet, Čangša, Kina
[b] Fakultet mašinstva i elektroenergetike, Univerzitet ,Tri klisure', Jičang, Kina

*Apstrakt*

*Da bi se simulirao normalan rast zrna čistog železa napravljen je trodimenzionalni (3D) model višefaznog polja. Napredna tehnologija vizualizacije je upotrebljena da bi se dobili podaci za pojedinačna zrna, što može jasno da pokaže morfologiju zrna sa jasno određenom površinom granice zrna kao i prostorni raspored susednih zrna. Na osnovu rezultata simulacije, opisan je model kinetike rasta zrna, koji je u skladu sa Burk i Tumbul paraboličnim zakonom. Ispitivani su fenomen ,Hilertovog režima' rasta zrna u 3D, kao i topološka transformacija mehanizma. Distribucija veličine zrna pod različitim vremenom evolucije pokazuje poklapanje sa Hilertovom distribucijom. Analizirani su detalji rasta zrna, posebno distribucija veličine zrna i obim stope rasta. Izvršeno je poređenje modela Nojmana Mulina i Hilgensfeldta za predviđanje volumetrijske stope rasta. Volumetrijska stopa rasta je približna nuli kada je broj strana zrna oko 13.7. Simulacija višefaznog polja se može koristiti za analizu dinamičke evolucije odnosa zrna, kao i za otkrivanje opšteg zakona normalnog rasta zrna kvantitativno.*

*Ključne reči: Rast zrna; Model višefaznog polja; Distribucija veličine zrna; Topološka analiza*